Seasonal variability of nitrous oxide concentrations and emissions along the Elbe estuary

Gesa Schulz[1,2], Tina Sanders[2], Yoana G. Voynova[2], Hermann W. Bange[3], and Kirstin Dähnke[2]

[1]Institute of Geology, Center for Earth System Research and Sustainability (CEN), University Hamburg, Hamburg, 20146, Germany
[2]Institute of Carbon Cycles, Helmholtz Centre Hereon, Geesthacht, 21502, Germany
[3]Marine Biogeochemistry Research Division, GEOMAR Helmholtz Centre for Ocean Research Kiel, Kiel, 24105, Germany

Correspondence to: Gesa Schulz (Gesa.Schulz@hereon.de)

Abstract

Nitrous oxide (N_2O) is a greenhouse gas, with a global warming potential 298 times that of carbon dioxide. Estuaries can be sources of N_2O, but their emission estimates have significant uncertainties due to limited data availability and high spatiotemporal variability. We investigated the spatial and seasonal variability of dissolved N_2O and N_2O emissions along the Elbe estuary (Germany). During nine research cruises done between 2017 and 2022, we measured dissolved N_2O concentrations, as well as dissolved nutrients and oxygen concentrations along the estuary and calculated N_2O saturation, flux densities and emissions. We found intense N_2O production along the Elbe estuary that compensated the effect of decreasing dissolved inorganic nitrogen (DIN) loads since the 1990s. Two hot-spots areas of N_2O production have been identified in the estuary: the Port of Hamburg and the mesohaline estuary near the estuarine turbidity maximum (MTZ). N_2O production was enhanced by warmer temperatures and fueled by riverine organic matter in the Hamburg Port or marine organic matter in the MTZ. Surprisingly, estuarine N_2O emissions where equally high in winter and summer. In winter, high riverine N_2O concentrations led to high N_2O emissions from the estuary, whereas in summer, estuarine biological N_2O production led to equally high N_2O emissions. Overall, we find that the Elbe estuary is a year-round source of N_2O with estimated annual emissions of 0.24 ± 0.06 Gg yr^{-1}.

1 Introduction

Nitrous oxide (N_2O) is an important atmospheric trace gas that contributes to global warming and stratospheric ozone depletion (WMO, 2018; IPCC, 2021). Estuaries are important regions of nitrogen turnover (Middelburg and Nieuwenhuize, 2001; Crossland et al., 2005; Bouwman et al., 2013), and a potential source of N_2O (Bange, 2006; Barnes and Upstill-Goddard, 2011; Murray et al., 2015). Together with coastal wetlands, estuaries contribute between 0.17 and 0.95 Tg N_2O-N of the annual global budget of 16.9 Tg N_2O-N (Murray et al., 2015; Tian et al., 2020). N_2O emission estimates from estuaries are associated with significant uncertainties due to limited data availability and high spatiotemporal variability (e.g. Bange 2006; Barnes and Upstill-Goddard 2011; Maavara et al. 2019), presenting a big challenge for the global N_2O emission estimates.

Nitrification and denitrification are the most important N_2O production pathways in estuaries. Under oxic conditions, N_2O is produced as a side product during the first step of nitrification, the oxidation of ammonia to nitrite (e.g. Wrage et al. 2001; Barnes and Upstill-Goddard 2011). At low oxygen (but not anoxic) conditions, nitrifier-denitrification may occur, during which nitrifiers reduce nitrite to N_2O (e.g. Wrage et al. 2001; Bange

1

39 2008). Denitrification takes place under anoxic conditions and mostly acts as a source of N_2O, but can also reduce

40 N_2O to N_2 (e.g. Knowles 1982; Bange 2008). In estuaries, denitrification mainly occurs in anoxic sediments

41 whereas oxic nitrification and nitrifier-denitrification take place in the oxygenated water column (e.g. Beaulieu et

42 al. 2011; Murray et al. 2015). Beside oxygen availability, temperature, substrate availability, pH and water level

43 can also control nitrous oxide production (Murray et al., 2015; Quick et al., 2019).

44 The Elbe estuary is a heavily managed estuary that hosts the third biggest port in Europe (e.g. Radach and Pätsch

45 2007; Bergemann and Gaumert 2010; Pätsch et al. 2010; Quiel et al. 2011). It has been identified as a N_2O source,

46 with a hotspot of N_2O production in the Port of Hamburg (Hanke and Knauth, 1990; Brase et al., 2017). However,

47 the seasonal variability of N_2O along the estuary is largely unknown so far. Therefore, the objectives of our study

48 were (1) to detect a long-term trend of N_2O concentrations, (2) to decipher the spatial and temporal distribution of

49 N_2O concentrations along the Elbe estuary during different seasons and (3) to identify hotspots and drivers for

50 N_2O production. To this end, we present here measurements of dissolved N_2O as well as dissolved nutrients and

51 oxygen from nine research cruises along the Elbe estuary from August 2017 to March 2022.

2 Methods

2.1 Study site

54 The Elbe River stretches over 1094 km from its spring in the Giant Mountains (Czech Republic) to the North Sea

55 (Cuxhaven, Germany). The catchment of the Elbe river is 140 268 km² (Boehlich and Strotmann, 2019), with 74 %

56 urban and agricultural land-use (Johannsen et al., 2008). This makes the Elbe the second largest German river

57 discharging into the North Sea, as well as the largest source of dissolved nitrogen for the German Bright, which is

58 heavily affected by eutrophication (van Beusekom et al., 2019).

59 The Elbe estuary begins at stream kilometer 586 at a weir in Geesthacht and flows through the Port of Hamburg,

60 entering the North Sea near Cuxhaven, stream kilometer 727 (Fig. 1). Estuaries are commonly structured along

61 their salinity gradient into an oligohaline section (salinity: 0.5 – 5.0), a mesohaline section (salinity: 5.0 – 18.0)

62 and polyhaline section (salinity > 18.0) (US EPA, 2006). The Elbe estuary has a length of 142 km (Boehlich and

63 Strotmann, 2019) and a mean annual discharge of 712 m³ s^{-1} with a mean variation range of 276 m³ s^{-1} to

64 1960 m³ s^{-1} (measured at gauge Neu Darchau at stream kilometer 536) (HPA and Freie und Hansestadt Hamburg,

65 2017). The average water residence time is ~32 days and ranges from ~72 days during low discharge (300 m³ s^{-1})

66 to ~10 days with high discharge (2000 m³ s^{-1}) (Boehlich and Strotmann, 2008). The estuary has an annual nitrogen

67 load of 84 Gg-N (FGG Elbe, 2018). Oxygen concentrations in the Elbe estuary shows a high seasonal variability:

68 In summer months, oxygen depletion and low oxygen zones occur regularly reaching concentrations below 3 mg

69 O_2 L^{-1} (Schroeder, 1997; Gaumert and Bergemann, 2007; Schöl et al., 2014).

70 The Elbe estuary is deepened and dredged on a regular basis to grant access for large container ships to the Port

71 of Hamburg (Boehlich and Strotmann, 2019), which is the third biggest port in Europe (HAFEN HAMBURG,

72 2021). Construction work for further deepening of the fairway was carried out in our study period, from 2019 to

73 early 2022.

Figure 1: Map of the Elbe estuary sampled during the research cruises with stream kilometers indicated (wsv.de, last access: 12.09.2022). Background map: © OpenStreetMap contributors 2021. Distributed under the Open Data Commons Open Database License (ODbL) v1.0. The Hamburg Port region stretches from stream kilometer 620 – 635 and is shown between the two grey dashed lines. The typical position of the maximum turbidity zone (MTZ) is shown between the dotted grey lines (Bergemann, 2004).

2.2   Transect sampling and measurements

We performed nine sampling campaigns along the estuary with the research vessel Ludwig Prandtl (Tab. 1). Most of the cruises took place during the spring and summer seasons, with water temperatures > 10 °C (May – September), while two cruises were conducted in colder winter months (early March, water temperature < 6 °C) (Tab. 1). Transect sampling started in the German Bright, close to the island Scharhörn and continued along the salinity gradient, through the Port of Hamburg to Oortkaten (stream kilometer 609). Transect sampling always was performed after high-tide, steaming upstream against the outgoing tide. For comparison, we included summer data from a previous study in 2015 (Brase et al., 2017).

Table 1: Campaign dates with the sampled Elbe estuary sections shown via stream kilometers, average discharge during each cruise measured at the Pegel Neu Darchau, averages and standard deviations for water temperature (°C), wind speed (m³ s⁻¹) in 10 m height, dissolved inorganic nitrogen (DIN) concentrations (µmol L⁻¹) for each campaign.

Campaign Dates	Stream kilometers (km)	Water temperature (°C)	Wind speed 10 m (m s⁻¹)	Average discharge (m³ s⁻¹)	Average DIN load (µmol L⁻¹)
28.-29.04.2015	627 – 741	12.3 ± 1.0	11.8 ± 0.3	595	191.0 ± 45.0
02.-04.06.2015	609 – 739	17.4 ± 1.7	5.0 ± 1.3	276	105.9 ± 36.2
01.-02.08.2017	621 – 749	20.9 ± 0.7	3.6 ± 1.5	607	$79.2 + 30.2$
04.-05.06.2019	610 – 750	18.7 ± 2.2	4.0 ± 1.7	423	108.3 ± 35.9
30.07.-01.08.2019	609 – 752	22.6 ± 1.0	4.2 ± 1.4	171	60.8 ± 38.6
19.-20.06.2020	609 – 747	19.8 ± 1.4	5.8 ± 1.2	331	74.6 ± 33.8
09.-11.09.2020	607 – 745	18.9 ± 0.6	5.9 ± 2.8	305	93.1 ± 32.7
10.-12.03.2021	609 – 748	5.4 ± 0.5	9.3 ± 2.6	862	324.4 ± 83.8
04.-05.05.2021	610 – 751	10.5 ± 0.8	11.0 ± 3.1	411	85.7 ± 36.6
27.-28.07.2021	621 – 751	22.2 ± 0.7	5.2 ± 1.3	721	139.8 ± 58.4
01.-02.03.2022	610 – 752	5.6 ± 0.2	2.9 ± 1.0	1282	238.0 ± 74.7

An onboard membrane pump continuously provided water from 1.2 m depth to an on-line in-situ FerryBox system and to an equilibrator used for the measurements of N_2O dry mole fraction (Section 2.4). The FerryBox system continuously measured water temperature, salinity, oxygen concentration, pH and turbidity. We corrected the oxygen measurements using the salinity corrected optode measurements in comparisons to Winkler titrations. The corrections of the individual cruises are listed in the Tab. S1 of the supplementary material.

Discrete water samples were taken every 20 min from a bypass of the FerryBox system. For nutrient analysis water samples were filtered immediately through combusted, pre-weighted GF/F Filters (4 h, 450 °C), and stored frozen in acid washed PE-bottles until analysis. The filters were stored frozen (-20 °C) and used for the later analysis of suspended particulate matter (SPM), particulate nitrogen fraction (PN), particulate carbon fraction (PC) and C/N ratios (supplementary material Fig. S1).

2.3 Nutrient measurements

Filtered water samples were measured in triplicates with a continuous flow auto analyzer (AA3, SEAL Analytics) using standard colorimetric and fluorometric techniques (Hansen and Koroleff 2007) for dissolved nitrate (NO_3^-), nitrite (NO_2^-) and ammonium (NH_4^+) concentrations.

2.4 Equilibrator based N_2O measurements and calculations

Equilibrated dry mole fractions of N_2O were measured by a N_2O analyzer based on off-axis integrated cavity output (OA-ICOS) absorption spectroscopy (Model 914-0022, Los Gatos Res. Inc., San Jose, CA, USA), which was coupled with a sea water/gas equilibrator using off-axis cavity output spectroscopy. Brase et al. (2017) described the set-up and instrument precision in detail. We regularly analyzed two standard gas mixtures of N_2O in synthetic air (500.5 ppb ± 5 % and 321.2 ppb ± 3 %) to validate our measurements. No drift was detected during our cruises.

112 We calculated the dissolved N_2O concentrations in water with the Bunsen solubility function of Weiss and Price

113 (1980) using 1 min averages of the measured N_2O dry mole fraction (ppb). Temperature differences between

114 sample inlet and equilibrator were taken into account for the calculation of the final N_2O concentrations (Rhee et

115 al., 2009). N_2O saturation were calculated based on N_2O concentrations in water (N_2O_{cw}) and in the air (N_2O_{air})

116 (Eq. 1). During each cruise, we regularly measured the atmospheric N_2O dry mole fractions.

$$s = 100 \times \frac{N_2O_{cw}}{N_2O_{air}} \tag{1}$$

117

118 The gas transfer coefficients (k) were determined based on Borges et al. (2004) taking the Schmidt number (Sc)

119 and wind speed in 10 m height (u_{10}) into account (Eq. 2). The Schmidt number was calculated as ratio of the

120 kinematic viscosity in water (Siedler and Peters, 1986) to the N_2O diffusivity in water (Rhee, 2000). Wind speeds

121 were measured on board in 10 m height of the *R/V Ludwig Prandtl* by a MaxiMet GMX600 (Gill Instruments

122 Limited). Flux densities were calculated according to Equation 3.

$$k = 0.24 \times (4.045 + 2.58u_{10}) \times \left(\frac{Sc}{600}\right)^{-0.5} \tag{2}$$

$$f = k \times (N_2O_{cw} - N_2O_{air}) \tag{3}$$

123 For emission calculations we used an area of 371.85 km² for the Elbe estuary in line with Brase et al. (2017). We

124 calculated seasonal averages for winter and spring/summer based on our transect cruises, which we used for

125 estimation of annual emissions.

2.5   Excess N_2O and apparent oxygen utilization

127 The correlation between excess N_2O (N_2O_{xs}) and apparent oxygen utilization (AOU) can provide insights into N_2O

128 production. We calculated N_2O_{xs} as the difference between the N_2O concentration in water (N_2O_w) and the

129 theoretical equilibrium concentration (N_2O_{eq}) (Eq. 4). AOU was determined using equation 5, where O_2 is the

130 measured dissolved oxygen concentration, and O_2' is the theoretical equilibrium concentration between water and

131 atmosphere calculated according to Weiss (1970).

$$N_2O_{xs} = N_2O_w - N_2O_{eq} \tag{4}$$

$$AOU = O_2' - O_2 \tag{5}$$

132 A linear relationship between AOU and N_2O_{xs} is usually an indicator for nitrification (Nevison et al., 2003; Walter

133 et al., 2004).

3   Results

3.1   Hydrographic properties and DIN distribution

136 Discharge ranged between 171 m³ s⁻¹ and 1282 m³ s⁻¹ during our cruises (ZDM, 2022), with higher discharge in

137 winter and lower discharge in summer (Tab. 1). Average water temperature over the entire estuary ranged from

138 5.4 ± 0.5 °C in March 2021 to 22.6 ± 1.0 °C in August 2017 (Tab. 1). For the further evaluation, March 2021 and

139 2022 cruises will be regarded as winter cruises (water temperature < 6°C), whereas all cruises with higher water

140 temperature are jointly regarded as spring and summer conditions.

141 Nitrate was the major form of dissolved inorganic nitrogen (DIN) during all cruises. In winter, high nitrogen

142 concentrations entered the estuary from the river. Towards summer, the riverine input (stream kilometer < 620)

143 decreased, but along the estuary nitrate concentrations increased up to approximate stream kilometer 700, then

144 decreased again towards the North Sea. Nitrate concentrations were highest during both March cruises with

145 averages of 319.0 ± 85.7 µmol L^{-1} and 230.9 ± 76.2 µmol L^{-1} in 2021 and 2022, respectively. During summer,

146 nitrate concentrations were lower. The nitrate concentrations averages were between 151.0 ± 58.1 µmol L^{-1} in May

147 2021 and 63.3 ± 38.8 µmol L^{-1} in July 2019 (Fig. 2a and b).

148 Nitrite and ammonium concentrations were usually low along the Elbe estuary, but showed peaks in the Hamburg

149 Port region and around stream kilometer 720 (Fig. 2c and 2e). We measured pronounced variations in nitrite

150 concentrations during most of our cruises, ranging from > 6.0 µmol L^{-1} (July 2019) to concentrations below the

151 detection limit (< 0.05 µmol L^{-1}) (Fig. 2c and d). The highest ammonium concentration was measured in March

152 2021 with 23.5 µmol L^{-1}. Over large stretches of the estuary, ammonium was below the detection limit

153 (< 0.07 µmol L^{-1}) in winter as well as in spring and summer (Fig. 2e and f).

154
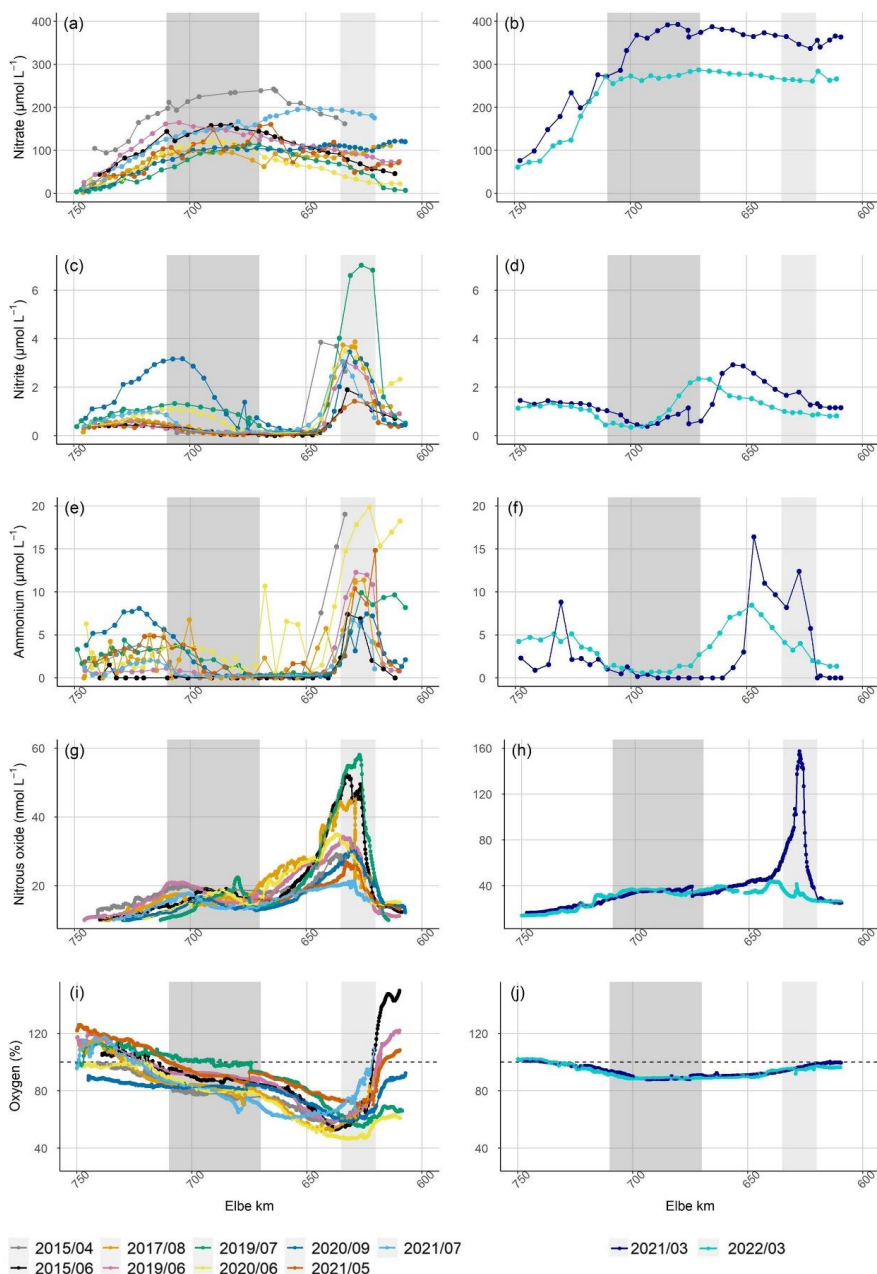
Figure 2: Nitrate concentration in µmol L^{-1} along the Elbe estuary (a) in spring/summer, (b) in winter. Nitrite concentration in µmol L^{-1} along the Elbe estuary (c) in spring/summer and (d) in winter. Ammonium concentration in µmol L^{-1} along the Elbe estuary (e) in spring/summer and (f) in winter. N$_2$O concentration in nmol L^{-1} along the Elbe estuary (g) in spring/summer, (h) in winter. Dissolved oxygen in % saturation along the Elbe estuary (i) in spring/summer and (j) in winter. All values are potted against stream kilometers. The Hamburg Port region is shown with light grey background. The typical position of the maximum turbidity zone (MTZ) is shown with a dark grey (Bergemann, 2004) Y-axis scales differ for the plots of N$_2$O concentrations (g) and (h). The dashed black lines in (i) and (j) indicate an oxygen saturation of 100 %.

3.2 Atmospheric and dissolved N₂O

The average atmospheric N_2O dry mole fractions ranged from 325 ppb in June 2015 to 336 ppb in July 2022 (Tab. 2). The differences between our measurements and the mean monthly N_2O mole fraction measured at the atmospheric monitoring station Mace Head (Ireland) (Dlugokencky et al., 2022) were always less than 1.5 %, indicating a good agreement with the monitoring data.

Comparable to the nutrient concentrations, N_2O varied seasonally (Fig. 2): In spring and summer, riverine N_2O (i.e., inflow into the estuary, stream kilometer <589) ranged from 8 nmol L^{-1} to 15 nmol L^{-1}. At the onset of the estuary, spring and summer N_2O concentrations usually showed a steep increase and peak values between 27 nmol L^{-1} and 58 nmol L^{-1} (~stream kilometer 620-635). Further downstream, N_2O concentrations decreased towards a local minimum (~ stream kilometer 670). A second peak was located along the salinity gradient at salinity ~ 5 (~ stream kilometer 680 - 700) ranging from 17 nmol L^{-1} to 22 nmol L^{-1}. N_2O concentrations dropped towards equilibrium concentrations of 8 – 12 nmol L^{-1} in the North Sea (Fig. 2g).

In winter, riverine N_2O concentrations were elevated (~ 25 nmol L^{-1}) compared to spring and summer riverine concentrations. In 2021, a steep increase of N_2O concentrations occurred in the Hamburg Port region, (stream kilometer 620 – 635) leading to exceptionally elevated N_2O concentrations of up to 158 nmol L^{-1} (Fig. 2h). In March 2022, N_2O increased to 44 nmol L^{-1} in this region. Further downstream, N_2O concentrations remained relatively constant at ~ 35 nmol L^{-1} during both cruises, and dropped to near equilibrium concentrations between stream kilometer 700 and the coastal ocean.

3.3 N₂O saturations and flux densities

During all cruises, the Elbe estuary was supersaturated in N_2O in the freshwater region (Fig. 3). The average N_2O saturation over the entire transect ranged between 146 % and 243 % with an overall average of 197 % for all cruises. Highest N_2O saturations occurred in the Hamburg Port region in spring and summer with an average N_2O peak of 402 % and a maximum supersaturation of 710 % in July 2019. The distribution of N_2O saturations during the winter cruises were significantly different: In March 2022, highest N_2O saturation (280 %) occurred at stream kilometer 640. In March 2021, in contrast, we found an extraordinarily high peak with a saturation of 1018 %. Between stream kilometer 680 and 720, a supersaturation of up to 277 % occurred in spring and summer months. Further towards the North Sea, N_2O saturation decreased, and approaching equilibrium with the atmosphere.

Biogeosciences
Discussions
Open Access
EGU

191
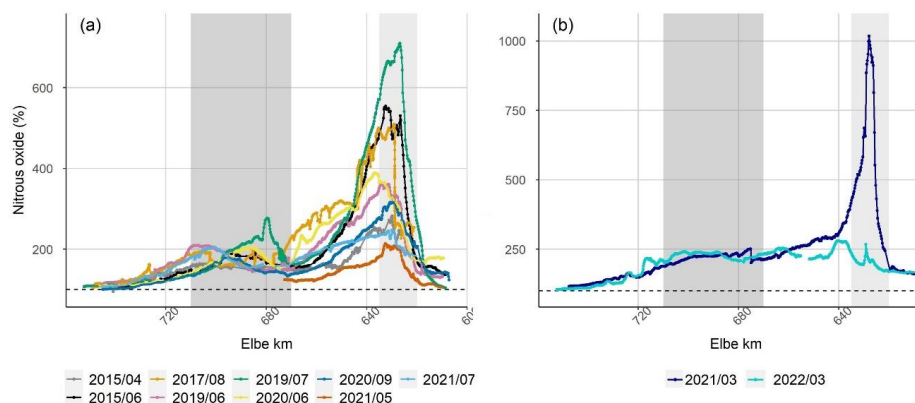
Figure 3: (a): N₂O saturation along the Elbe estuary for cruises in spring/summer, (b) N₂O saturation for the cruises done in March. The dashed black lines in both plots indicate a saturation of 100 %. The Hamburg Port region is shown with a background in light grey. The typical position of the maximum turbidity zone (MTZ) is shown with a dark grey (Bergemann, 2004). Y-axis scales differ for both plots.

196   The N₂O flux densities were usually highest in the Hamburg Port area with an average of 95.1 ± 113.6 µmol m^{-2}

197   d^{-1} and lowest towards the North Sea with an average of 3.9 ± 3.0 µmol m^{-2} d^{-1} (stream kilometers > 735). The

198   average N₂O flux density of all cruises was 37.8 ± 51.0 µmol m^{-2} d^{-1}. (Tab. 2).

199   **Table 2: Calculated average N₂O saturation, sea-to-air fluxes and atmospheric N₂O dry mole fractions during our**
200   **cruises for the Elbe estuary**

Campaign Dates	Average saturation (%)	N₂O Flux densities (µmol m^{-2} d^{-1})			Average atmospheric dry mole fraction (ppb)
		Min	Max	Average	
28.-29.04.15	160.8	-2.5	100.0	33.1 ± 21.0	331
02.-04.06.15	203.8	2.6	199.8	45.5 ± 49.8	325
01.-02.08.17	221.3	1.5	121.9	35.8 ± 31.8	331
04.-05.06.19	192.9	3.4	63.4	26.6 ± 16.1	332
30.07.-01.08.19	228.6	1.3	196.0	41.7 ± 49.7	327
19.-20.06.20	194.1	3.7	119.6	38.9 ± 30.8	330
09.-11.09.20	163.9	-0.1	60.3	21.1 ± 15.7	331
10.-12.03.21	244.2	9.1	745.7	105.6 ± 119.2	331
04.-05.05.21	123.5	-0.5	77.7	15.1 ± 19.9	331
27.-28.07.21	174.8	2.5	70.2	27.4 ± 14.7	336
01.-02.03.22	196.5	1.1	51.0	27.3 ± 13.6	333

201   **3.4   Dissolved oxygen saturation**

202   Average oxygen saturation varied between 76 and 95 in % saturation with a minimum in the Hamburg Port area.

203   Winter cruises showed only little variation, with oxygen remaining relatively constant along the estuary (> 88 %

204   saturation). During most spring and summer cruises, water from the river coming into the estuary was high in

205   oxygen. In the Hamburg Port region, oxygen saturation generally decreased. Lowest values occurred in June 2020

206   with 47 % saturation. The along-estuary minimum oxygen in summer months (June - August) was always below

9

207   61 % saturation. In spring and summer, oxygen increased towards the North Sea and reached 100 % saturation

208   (Fig. 2i and j).

209   Plots of excess N_2O (N_2O_{xs}) and apparent oxygen utilization (AOU) (Fig. 4) revealed excess N_2O along the entire

210   estuary (Fig. 4 and supplementary material S2). During all cruises, elevated riverine N_2O_{xs} concentrations entered

211   the estuary (stream kilometer < 620). In spring and summer, steep, non-linear increases of N_2O_{xs} in the Port of

212   Hamburg suggested in-situ N_2O production (Fig. 4a, 4b). This production extended into the oligohaline estuary

213   (stream kilometer > 635 and salinity < 5) followed by a linear decrease of N_2O_{xs} reduction in the transition region

214   to the mesohaline section of the estuary (salinity: 5-18), N_2O_{xs} increased again, followed by a decrease to 0 nmol

215   L^{-1} towards the North Sea. In winter, we found a linear relationship of N_2O_{xs} and AOU along the estuary, with a

216   decoupling in the Hamburg Port and the oligohaline part of the Elbe estuary. In Figure 4, representative

217   N_2O_{xs}/AOU plots for summer (4 a, b) and winter (4 c, d) are shown (see supplementary material: Fig. S2 for all

218   plots).

219
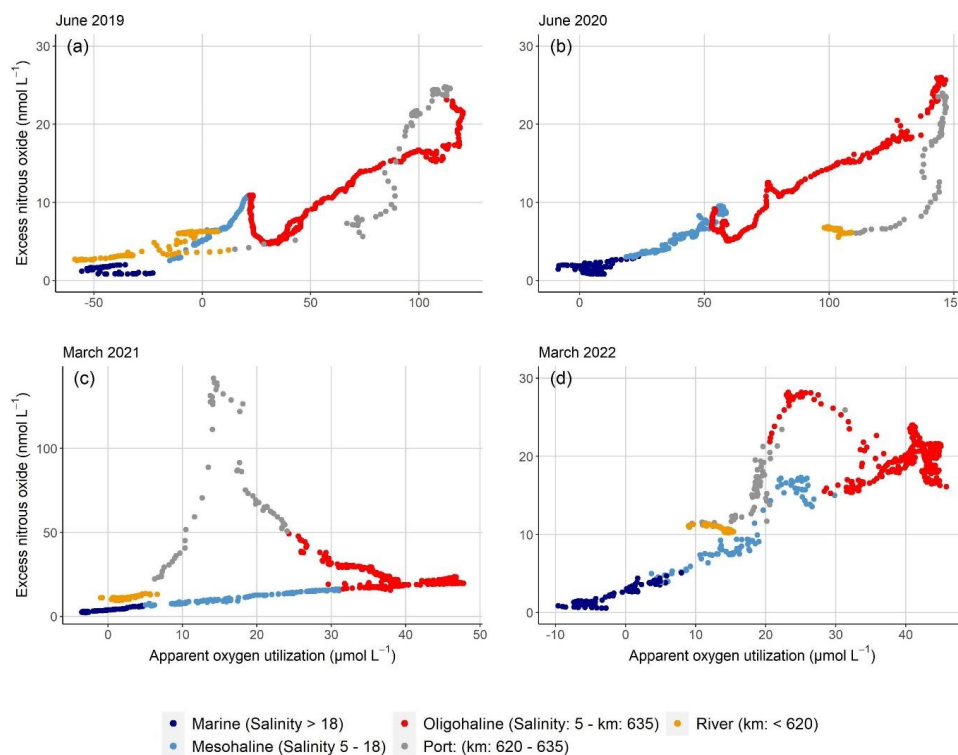
Figure 4: Representative plots of N_2O_{xs} vs AOU for (a) June 2019, (b) June 2020, (c) March 2021 and (d) March 2022.
The values are colored to distinguish between different regions of the estuary. Values upstream of stream kilometer 620
are yellow. In the Hamburg Port region (km: 620 – 635), points are colored grey. Red points mark the region
downstream of the port with low salinity (km: 635 – salinity 5). Up to stream kilometer 720, points are light blue
(mesohaline part, salinity: 5 – 18) and everything further out in the North Sea is a dark blue (salinity > 18). Y-axis scale
differ for Fig. 4c.

4   Discussion

4.1   N$_2$O saturation and flux densities of the Elbe estuary

226

227

228   The average N$_2$O saturation and flux density were 197 % and 39.68 µmol m^{-2} d^{-1}, respectively. The N$_2$O flux

229   densities from the Elbe estuary were in the mid-range of flux densities of other European estuaries ranging from

230   2.9 µmol m^{-2} d^{-1} to 96.5 µmol m^{-2} d^{-1} (e.g. Garnier et al. 2006; Gonçalves et al. 2010; Murray et al. 2015). But they

231   were significantly lower than observed medians for tidal environments with high DIN loads (72 µmol m^{-2} d^{-1} and

232   168 µmol m^{-2} d^{-1}) (Murray et al., 2015). As shown in Fig. 4, there was no linear relationship between N$_2$O$_{xs}$ and

233   AOU for most of the regions of the Elbe estuary. Therefore, large sections in the estuary were influenced by either

234   initial riverine N$_2$O production, or in-situ production along the estuary. During spring and summer, we found

235   enhanced N$_2$O concentrations in two regions: the Hamburg Port region (see also Brase et al. (2017)), and the

236   salinity gradient (stream kilometer 680 – 700, salinity ~5). Both N$_2$O peaks varied in height and spatial extension

237   suggesting in-situ biological production (Fig. 2g, 3a). This matches previous research linking estuarine N$_2$O fluxes

238   to in-situ generation (e.g. Bange 2006; Barnes and Upstill-Goddard 2011; Murray et al. 2015).

239   Previous measurements of N$_2$O saturation and flux densities in the Elbe estuary between the 1980s and 2015

240   (Hanke and Knauth, 1990; Barnes and Upstill-Goddard, 2011; Brase et al., 2017) showed a significant reduction

241   of N$_2$O saturation due to the reduced riverine nutrient load and higher dissolved oxygen concentrations (Brase et

242   al., 2017). Since the BIOGEST study in 1997 (Barnes and Upstill-Goddard, 2011), N$_2$O saturation did not decrease

243   in scale with riverine nitrogen input suggesting that in-situ N$_2$O production along the estuary is important (Fig. 5).

244   In the following sections, we investigate the biogeochemical controls of this in-situ production. For this purpose,

245   we discuss both zones of intense N$_2$O production separately and also distinguish between biological active cruises

246   in spring and summer (water temperature > 10 °C) and winter (water temperature < 6 °C).
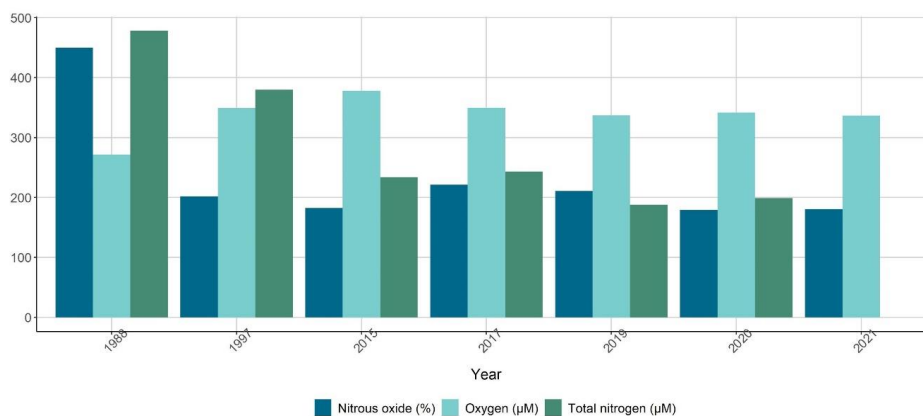
247

248   **Figure 5: Comparison of average N$_2$O saturation transect measurements with previous research from the Elbe estuary.**

249   **Average annual oxygen concentration and total nitrogen concentration are shown for the station Zollenspieker at the**

250   **beginning of the estuary (stream kilometer 598.7) and publicly available (Das Fachinfomrationssystem (FIS) der FGG**

251   **Elbe, 2022).Values for 2022 and total nitrogen concentration for 2021 are not presented as the data is not publicly**

252   **available yet.**

4.2   N$_2$O production in spring and summer in the mesohaline estuary

253

254   The N$_2$O peak in the transition between oligohaline and mesohaline estuary was accompanied by a sudden change

255   from a decreasing to an increasing trend between AOU and N$_2$O$_{xs}$, (Fig. 4a, 4b), pointing towards N$_2$O production

256   in the oxic water column. Interestingly, we find that small peaks of nitrite and ammonium coincided with the

257   nitrous oxide peak between km 680 -700, with ammonium around stream kilometer ~720, and a nitrite peak at

258   ~700. Highest N_2O concentrations were usually measured between the nitrite peak and the region with highest

259   turbidity (see Fig. 6 for an example, supplementary material Fig. S3-S13), as seen for our cruise in September

260   2020 in Fig. 6a. Such a succession of nitrite and ammonium peaks is typical for remineralization and nitrification,

261   and the slight decrease of oxygen concentrations around the N_2O peak (Fig. 2g and i) suggests that oxygen

262   consumption, possibly caused by nitrification, occured. Sanders et al. (2018) measured small but detectable

263   nitrification rates of $1 – 2$ µmol L^{-1} d^{-1} for this region of the Elbe estuary, suggesting that N_2O in this region may

264   be a side product of nitrification.
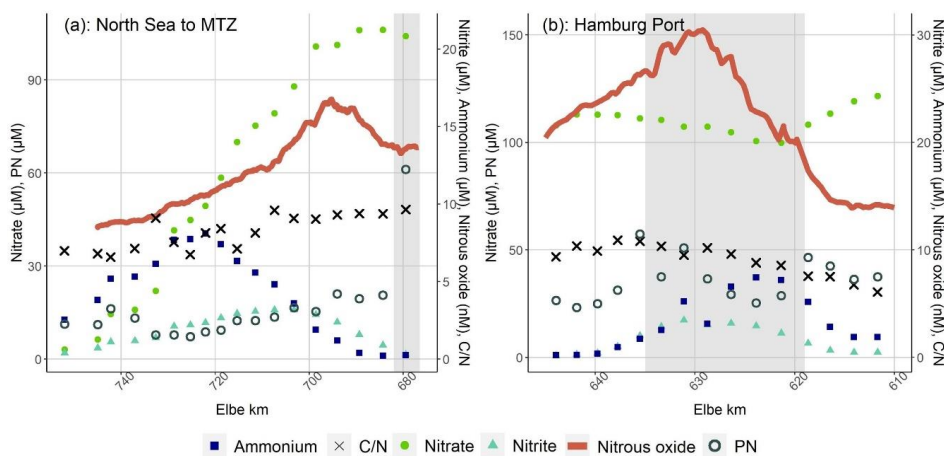
265
266   **Figure 6: (a) Succession of N-bearing substances coming from the North in September 2020. The grey area shows the**
267   **position of the MTZ. (b) Succession of N-bearing substances in the Port of Hamburg in September 2020. The grey area**
268   **shows the position of the Port of Hamburg. On the left y-axis nitrate concentrations in µmol L^{-1} are presented as green**
269   **circles and particulate nitrogen (PN) concentrations as unfilled circles in µmol L^{-1}. The right y-axis shows nitrite**
270   **concentrations in µmol L^{-1} as light blue triangles, ammonium concentration in µmol L^{-1} as dark blue squares, nitrous**
271   **oxide concentration in nmol L^{-1} as a red line and C/N ratios as grey crosses.**

272   However, this suggest input of particulate matter from the North Sea and upstream particle transport towards the

273   maximum turbidity zone of the estuary (MTZ). This transport mechanism is in line with Wolfstein and Kies (1999),

274   who explained organic matter contents and chlorophyll a concentrations in the polyhaline part of the Elbe estuary

275   by input of fresh marine particulate matter. Generally, the occurrence of an MTZ is unique to each estuary and is

276   generated by the balance between river-induced flushing and upstream transport of marine SPM as well as a

277   function of estuarine geomorphology, gravitational circulation and tidal flow, trapping the particles in the MTZ

278   (Bianchi, 2007; Sommerfield and Wong, 2011; Winterwerp and Wang, 2013). Other studies detected N_2O

279   production from water column nitrification in estuarine MTZs (e.g. Barnes and Owens 1999; de Wilde and de Bie

280   2000; Bange 2006; Barnes and Upstill-Goddard 2011; Harley et al. 2015), caused by high bacterial numbers,

281   particulate nitrogen availability and long residence times (Murray et al., 2015).

282   For the selected dataset, we calculated a negative correlation between average SPM concentrations and N_2O

283   saturation (R = -0.81), and found that the N_2O peak was located downstream of the MTZ, and upstream of

284   increasing nitrite and ammonium concentrations (Fig. 6). This (1) suggests that the mere concentration of SPM is

285   not the driving factor of nitrification as a source of N_2O, but that organic matter quality is key to biological turnover

286   (Dähnke et al. 2022), and (2) speaks in favor of material transport from the North Sea upstream towards the MTZ

287 (Kappenberg and Fanger, 2007). We find organic matter with low C/N ratios, and with relatively high PN and PC

288 contents in the outermost samples (ranging from 5.9 in June 2020 to 8.8 August 2017), indicating fresh and easily

289 degradable organic matter (supplementary material Fig. S1, e.g. Redfield et al. 1963; Fraga et al. 1998; Middelburg

290 and Herman 2007). Towards the MTZ, C/N values, PN and PC contents decreased, indicating remineralization in

291 the water column. This remineralization and subsequent nitrification can then cause the observed succession of

292 ammonium, nitrite and N_2O peaks (Fig. 6), contributing to the already high nitrate concentrations in the MTZ

293 coming from the upper estuary, where high C/N values (9 – 11/16) indicate low organic matter quality (e.g.

294 Hedges and Keil 1995; Middelburg and Herman 2007).

295 Overall, we conclude that remineralization of marine organic matter, followed by nitrification, produced the N_2O

296 peak in the salinity gradient of the Elbe estuary. This production was mainly fueled by fresh organic matter entering

297 the estuary from the North Sea.

4.3   Hamburg Port: N_2O production in spring and summer

299 Several studies identified the Hamburg Port region as a hotspot of biogeochemical turnover: Deek et al. (2013)

300 showed ongoing denitrification, Sanders et al. (2018) measured intense nitrification, Norbisrath et al. (2022)

301 determined intense total alkalinity generation, and Dähnke et al. (2022) found that nitrogen turnover were driven

302 by particulate organic matter. The highest N_2O peaks of our study were located in the Port of Hamburg. Brase et

303 al. (2017) identified the port region as a hotspot of N_2O production and hypothesized that simultaneous nitrification

304 and denitrification were responsible. We use our expanded dataset to further evaluate this hypothesis.

305 During all our cruises in spring and summer, we measured ammonium and nitrite peaks in the Hamburg Port region

306 (Fig. 2c and e, exemplary for September 2020 in Fig. 6b). High nitrite concentrations are favorable of N_2O

307 production by nitrification and of nitrifier-denitrification (Quick et al., 2019), and low-oxygen conditions made

308 both nitrification and denitrification plausible in this region. We found N_2O saturations increased with decreasing

309 discharge (R = -0.48) during spring and summer. This further points towards in-situ N_2O production, because

310 denitrification and nitrification are more intense at higher residence times (e.g. Nixon et al. 1996; Pind et al. 1997;

311 Silvennoinen et al. 2007; Gonçalves et al. 2010). Overall, our data show that the correlations of ammonium, nitrite

312 and N_2O are significant and confirm that simultaneous denitrification and nitrification likely are responsible for

313 N_2O production.

314 A correlation analysis for the Hamburg Port region (stream kilometer 610 – 645) revealed a strong negative

315 correlation of N_2O saturation with pH (R = -0.60), nitrite concentrations (R = 0.58), oxygen saturation (R = -0.58),

316 particulate carbon (PC) content (R = -0.53) and particulate nitrogen (PN) content (R = -0.49).

317 In spring and summer, we found no linear relationship of N_2O_{xs} and AOU in the Hamburg Port. This may result

318 from combined N_2O production by nitrification and denitrification. However, oxygen saturation and N_2O

319 saturation were inversely correlated in the Hamburg Port (R = -0.58), suggesting that N_2O production was

320 controlled by oxygen concentrations, and thus by oxygen consumption in the port region. Most (75 %) of this

321 oxygen consumption is caused by respiration (Schöl et al., 2014; Sanders et al., 2018). This respiration in turn is

322 determined by remineralization of algal material from the upstream river that is transported to and respired within

323 the port region (Schroeder, 1997; Kerner, 2000; Schöl et al., 2014), and this directly links estuarine N_2O production

324 to river eutrophication. Fresh organic matter from the Elbe River entered the estuary, showing up in low C/N

325 values ranging from 6.6 in July 2019 to 10.8 in August 2017 as well as in high PN and high PC contents, where it

326 rapidly got degraded in the Hamburg Port region (supplementary material Fig. S1). Dähnke et al. (2022) found

Biogeosciences
Discussions

327   labile organic matter strongly fueled nitrification but also denitrification in the fresh water part of the Elbe estuary,

328   which, as shown in our study, results in high N_2O production in the Hamburg Port region leading to the reported

329   negative correlations of PC and PN content with N_2O saturation.

330   Overall in spring and summer, oxygen conditions mainly controlled N_2O production in the Hamburg Port region.

331   Since respiration of organic matter dominates oxygen drawdown in the port region, we deduced that N_2O

332   production was linked to the decomposition of phytoplankton produced in the upstream Elbe river regions.

4.4   Hamburg Port: N_2O production in winter

334   Intriguingly, we also find high N_2O concentrations in the port region in winter, at a time when low water

335   temperature should hamper biological production. In the MTZ, the other identified region of intense estuarine N_2O

336   production, we did not detect an N_2O peak during either March cruise. With water temperature below 6 °C,

337   biological processing likely was inhibited (Koch et al., 1992; Halling-Sorensen and Jorgensen, 1993). For March

338   2022, we found a linear increase of N_2O_{xs} and AOU along with oxygen consumption and increasing ammonium,

339   nitrite and PN concentrations indicating nitrification in the port region producing N_2O. Unlike in summer, N_2O

340   concentrations showed a flat increase extending far into the oligohaline section of the estuary (Fig. 2, 4d,

341   supplementary material Fig. S1).

342   However, in March 2021, we found a sharp and sudden increase in N_2O, with a peak concentration that by far

343   exceeded internal biological sources in summer (Fig. 2h). Also, an ammonium peak in the water column coincided

344   with the N_2O maximum (Fig. 2f and supplementary material Fig. S10). If microbial activity is mostly temperature-

345   inhibited, a point source of N_2O in the port seems the most likely cause. Ammonium and N_2O concentrations are

346   high in the pore water of underlying sediments, so one potential source of elevated N_2O may be the deepening and

347   dredging works in the Hamburg Port region, stirring up sediment. Indeed, deepening and dredging work occurred

348   in the Hamburg Port region in 2021 (HPA, pers. Comm., Karrasch 2022). However, this also applied to 2022,

349   when we saw no sharp N_2O peak (Fig. 2h). Furthermore, the regions of deepening and dredging operation did not

350   match the region of high N_2O concentrations, and since turbidity at the time of sampling did not change

351   significantly compared to other cruises, this also speaks against a major signal from channel dredging and

352   deepening. Thus, we conclude that sediment input most likely was not the source of N_2O in the water column in

353   winter 2021.

354   Another possible source of N_2O is the waste water treatment plant (WWTP) Köhlbrandhöft, which treats the waste

355   water from the Hamburg metropolitan region. The WWTP outflow in the Southern Elbe joins the sampled stretch

356   at stream kilometer 626 (Fig. 1), matching the N_2O peak at stream kilometer 627 (Fig. 2h and 3b). We indeed

357   found out that aggravated operation conditions in the WWTP at the time of sampling were caused by an extreme

358   rain event on March 11th 2021 (HAMBURG WASSER, pers. Comm., Laurich 2022). While the operators could

359   still meet the limits for the effluent levels of nitrate and ammonium, higher than usual ammonium loads left the

360   treatment plant during the March 2021 campaign. We assume this elevated ammonium loads from the WWTP

361   most likely was the cause of the unexpected high N_2O peak in March 2021. Therefore, we argue that our March

362   2021 cruise likely represents an exception due to an extreme weather situation, and that typical winter conditions

363   in the Elbe estuary comply with the N_2O production, as in March 2022.

4.5 Seasonal changes of N$_2$O emissions

365 For an accurate assessment of annual estuarine N$_2$O emissions, we first evaluate their seasonal distribution. In

366 March, average N$_2$O emissions were 0.28 ± 0.17 Gg yr^{-1}. Note that we deliberately excluded the N$_2$O peak in

367 March 2021 and interpolated the concentrations in this region to exclude the effect of a point source (Section 4.4).

368 Nonetheless, high wind speeds still led to high N$_2$O emissions in March 2021 (Tab. 3). March 2022 (0.16 ± 0.08

369 Gg yr^{-1}) only slightly deviated from average N$_2$O emissions in spring and summer (0.20 ± 0.05 Gg yr^{-1}). Overall,

370 we calculated average annual emissions using the seasonal averages (Tab. 3) resulting in 0.24 ± 0.06 Gg yr^{-1}, thus

371 exceeding the recent summer N$_2$O emission estimates of 0.18 ± 0.01 Gg yr^{-1} by Brase et al. (2017).

372 Enhanced microbial N$_2$O production can lead to high N$_2$O flux densities in summer (Usui et al., 2001; Allen et al.,

373 2011; Murray et al., 2015; Quick et al., 2019), as is the case for the Elbe estuary in spring and summer (Fig. 7).

374 However, winter flux densities were unexpectedly high (Fig. 7). Elevated winter N$_2$O emissions originated from

375 1) high wind speeds with increased sea-air exchange, 2) nitrification in the Hamburg Port and 3) elevated riverine

376 N$_2$O inputs into the estuary, with 25 nmol L^{-1} (161.9 % saturation) and 26 nmol L^{-1} (165.3 % saturation) in March

377 2021 and 2022, respectively, well above summer riverine input concentrations. Since the Elbe estuary acted as a

378 transport channel, rather than a bioreactor in the winter months, due to temperature inhibited biological processing

379 (Koch et al., 1992; Halling-Sorensen and Jorgensen, 1993), the N$_2$O concentrations remained high until mixing

380 with water from the North Sea, which resulted in a decrease and in outgassing to the atmosphere.
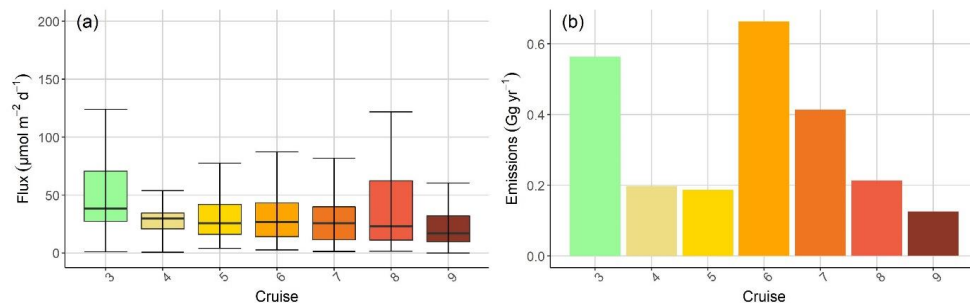
381

382 **Figure 7: (a) Monthly variation of N$_2$O flux density in µmol m^{-2} d^{-1}, (b) monthly variation of N$_2$O emissions in Gg yr^{-1}.**

383 The high riverine N$_2$O input into the estuary is intriguing and may be caused by high nitrate discharge from soils

384 and groundwater fueling N$_2$O production, which was found in other streams and rivers (Beaulieu et al., 2009;

385 Clough et al., 2011). Agricultural fertilizer application might also affect winter N$_2$O concentrations (Murray et al.,

386 2015), since it can lead to high DIN and N$_2$O concentrations in estuaries. In the 1990s, Hanke and Knauth (1990)

387 also measured high riverine N$_2$O concentrations in the Elbe estuary in winter, albeit at higher DIN concentrations.

388 Other temperate estuaries showed high N$_2$O emissions with the dominant control on N$_2$O concentrations being

389 freshwater delivery, rather than in-situ production (Barnes and Owens, 1999; Robinson et al., 1998; Murray et al.,

390 2020). In combination with a higher probability of strong winds in winter, it is clear that winter N$_2$O emissions in

391 the Elbe estuary should not be neglected, as they can potentially even exceed summer emissions.

392 Overall in winter, large nitrogen loads from the Elbe catchment caused high riverine N$_2$O concentrations, which

393 led to high N$_2$O emissions in the adjacent estuary (Fig. 7). In summer, reduced riverine N$_2$O input was compensated

394 by in-situ N$_2$O production processes. We find that both effects are currently balanced, leading to year-round high

395 N$_2$O emissions in this estuary.

396 **Table 3: Average N$_2$O flux densities and emissions for spring and summer, winter and per year. For the winter, only**
397 **the March 2022 cruise was used due to the extreme peak in 2021 that was most probably caused by a point-source influx**
398 **of ammonium and an extreme weather event. For the emissions calculation, the area of the Elbe estuary of 371.85 km²**
399 **was taken into account (Brase et al., 2017).**

Season	Average N$_2$O flux densities	N$_2$O emissions
Spring and summer	33.5 ± 7.8 µmol m^{-2} d^{-1}	0.20 ± 0.05 Gg yr^{-1}
March	47.3 ± 28.1 µmol m^{-2} d^{-1}	0.28 ± 0.17 Gg yr^{-1}
Annual average	40.3 ± 14.3 µmol m^{-2} d^{-1}	0.24 ± 0.06 Gg yr^{-1}

400 ## 5   Conclusions

401 Overall, we found enhanced N$_2$O concentrations along the entire Elbe estuary, which point towards in-situ N$_2$O
402 production that compensated the effect of decreasing DIN loads since the 1990s. Two hot-spots of N$_2$O production
403 were found in the estuary: the Port of Hamburg and the mesohaline estuary near the estuarine turbidity maximum.
404 Biological N$_2$O production was enhanced by warmer temperatures and fueled by riverine organic matter in the
405 Hamburg Port or marine organic matter in the MTZ.

406 We saw no seasonality in N$_2$O emissions, despite seasonal variations in in-situ N$_2$O production: In winter, high
407 riverine N$_2$O input led to high N$_2$O saturation and emissions in the estuary, whereas in summer, high N$_2$O emissions
408 were controlled by in-situ production. Overall, the Elbe estuary is a year-round perennial source of N$_2$O, with
409 estimated annual emissions of 0.24 ± 0.06 Gg yr^{-1}. In conjunction with the overarching control of N$_2$O production
410 by organic matter quality, this highlights that a holistic approach of water quality improvement and nutrient
411 mitigation is needed to further reduce N$_2$O emission from the Elbe estuary.

412 **Data availability**

413 The dataset generated and/or analyzed in this study are currently available upon request from the corresponding
414 author and will be made publicly available under coastMap Geoportal (www.coastmap.org) connecting to
415 PANGAEA. (https://www.pangaea.de/) with DOI availability in the near future.

416 **Authors contribution**

417 GS, TS and KD designed this study. GS did the sampling and measurements for cruises from 2020 to 2022 as well
418 as the data interpretation and evaluation. TS was responsible for the sampling and measurements for cruises done
419 in 2017 and 2019. YGV provided the oxygen data correction from the FerryBox data. KD, HWB, YGV and TS
420 contributed with scientific and editorial recommendations. GS prepared the manuscript with contributions of all
421 co-authors.

422 **Competing interest**

423 The authors declare that they have no conflict of interest.

References

Allen, D., Dalal, R. C., Rennenberg, H., and Schmidt, S.: Seasonal variation in nitrous oxide and methane
emissions from subtropical estuary and coastal mangrove sediments, Australia, Plant Biol., 13, 126–133,
https://doi.org/10.1111/j.1438-8677.2010.00331.x, 2011.

Bange, H. W.: Nitrous oxide and methane in European coastal waters, Estuar. Coast. Shelf Sci., 70, 361–374,
https://doi.org/10.1016/j.ecss.2006.05.042, 2006.

Bange, H. W.: Chapter 2 - Gaseous Nitrogen Compounds (NO, N_2O, N_2, NH_3) in the Ocean, in: Nitrogen in the
Marine Environment (Second Edition), edited by: Capone, D. G., Bronk, D. A., Mulholland, M. R., and Carpenter,
E. J., Academic Press, San Diego, 51–94, https://doi.org/10.1016/B978-0-12-372522-6.00002-5, 2008.

Barnes, J. and Owens, N. J. P.: Denitrification and Nitrous Oxide concentrations in the Humber Estuary, UK, and
Adjacent Coastal Zones, Mar. Pollut. Bull., 37, 247–260, https://doi.org/10.1016/S0025-326X(99)00079-X, 1999.

Barnes, J. and Upstill-Goddard, R. C.: N_2O seasonal distributions and air-sea exchange in UK estuaries:
Implications for the tropospheric N_2O source from European coastal waters, J. Geophys. Res. Biogeosciences,
116, https://doi.org/10.1029/2009JG001156, 2011.

Beaulieu, J. J., Arango, C. P., and Tank, J. L.: The Effects of Season and Agriculture on Nitrous Oxide Production
in Headwater Streams, J. Environ. Qual., 38, 637–646, https://doi.org/10.2134/jeq2008.0003, 2009.

Beaulieu, J. J., Tank, J. L., Hamilton, S. K., Wollheim, W. M., Hall, R. O., Mulholland, P. J., Peterson, B. J.,
Ashkenas, L. R., Cooper, L. W., Dahm, C. N., Dodds, W. K., Grimm, N. B., Johnson, S. L., McDowell, W. H.,
Poole, G. C., Valett, H. M., Arango, C. P., Bernot, M. J., Burgin, A. J., Crenshaw, C. L., Helton, A. M., Johnson,
L. T., O'Brien, J. M., Potter, J. D., Sheibley, R. W., Sobota, D. J., and Thomas, S. M.: Nitrous oxide emission
from denitrification in stream and river networks, Proc. Natl. Acad. Sci., 108, 214–219,
https://doi.org/10.1073/pnas.1011464108, 2011.

Bergemann, M.: Die Trübungszone in der Tideelbe - Beschreibung der räumlichen und zeitlichen Entwicklung,
Wassergütestelle Elbe, 2004.

Bergemann, M. and Gaumert, T.: Elbebericht 2008, Flussgebietsgemeinschaft Elbe, Hamburg, 2010.

Bianchi, T. S.: Biogeochemistry of Estuaries, Oxford University Press, New York, 706 pp., 2007.

Boehlich, M. J. and Strotmann, T.: The Elbe Estuary, Küste, 74, 288–306, 2008.

464 Boehlich, M. J. and Strotmann, T.: Das Elbeästuar, Küste, 87, Kuratorium für Forschung im Küsteningenieurwesen
465 (KFKI), https://doi.org/10.18171/1.087106, 2019.

466 Borges, A., Vanderborght, J.-P., Schiettecatte, L.-S., Gazeau, F., Ferrón-Smith, S., Delille, B., and Frankignoulle,
467 M.: Variability of gas transfer velocity of CO_2 in a macrotidal estuary (The Scheldt), Estuaries, 27, 593–603,
468 https://doi.org/10.1007/BF02907647, 2004.

469 Bouwman, A. F., Bierkens, M. F. P., Griffioen, J., Hefting, M. M., Middelburg, J. J., Middelkoop, H., and Slomp,
470 C. P.: Nutrient dynamics, transfer and retention along the aquatic continuum from land to ocean: towards
471 integration of ecological and biogeochemical models, Biogeosciences, 10, 1–22, https://doi.org/10.5194/bg-10-1-
472 2013, 2013.

473 Brase, L., Bange, H. W., Lendt, R., Sanders, T., and Dähnke, K.: High Resolution Measurements of Nitrous Oxide
474 (N_2O) in the Elbe Estuary, Front. Mar. Sci., 4, 162, https://doi.org/10.3389/fmars.2017.00162, 2017.

475 Clough, T. J., Buckthought, L. E., Casciotti, K. L., Kelliher, F. M., and Jones, P. K.: Nitrous oxide dynamics in a
476 braided river system, New Zealand, J. Environ. Qual., 40, 1532–1541, https://doi.org/10.2134/jeq2010.0527, 2011.

477 Crossland, C. J., Baird, D., Ducrotoy, J.-P., Lindeboom, H., Buddemeier, R. W., Dennison, W. C., Maxwell, B.
478 A., Smith, S. V., and Swaney, D. P.: The Coastal Zone — a Domain of Global Interactions, in: Coastal Fluxes in
479 the Anthropocene: The Land-Ocean Interactions in the Coastal Zone Project of the International Geosphere-
480 Biosphere Programme, edited by: Crossland, C. J., Kremer, H. H., Lindeboom, H. J., Marshall Crossland, J. I., and
481 Le Tissier, M. D. A., Springer, Berlin, Heidelberg, 1–37, https://doi.org/10.1007/3-540-27851-6_1, 2005.

482 Dähnke, K., Sanders, T., Voynova, Y., and Wankel, S. D.: Nitrogen isotopes reveal a particulate-matter-driven
483 biogeochemical reactor in a temperate estuary, Biogeosciences, 19, 5879–5891, https://doi.org/10.5194/bg-19-
484 5879-2022, 2022.

485 Deek, A., Dähnke, K., van Beusekom, J., Meyer, S., Voss, M., and Emeis, K.-C.: N_2 fluxes in sediments of the
486 Elbe Estuary and adjacent coastal zones, Mar. Ecol. Prog. Ser., 493, 9–21, https://doi.org/10.3354/meps10514,
487 2013.

488 Dlugokencky, E. J., Crotwell, A. M., Mund, J. W., Crotwell, M. J., and Thoning, K. W.: Earth System Research
489 Laboratory Carbon Cycle and Greenhouse Gases Group Flask-Air Sample Measurements of N_2O at Global and
490 Regional Background Sites, 1967-Present [Data set], https://doi.org/10.15138/53G1-X417, 2022.

491 FGG Elbe, Flussgebietsgemeinschaft Elbe: Naehrstoffminderungsstrategie für die Flussgebietsgemeinschaft Elbe,
492 Gemeinsamer Bericht der Bundesländer und der Flussgebietsgemeinschaft Elbe, 2018.

493 Das   Fachinfomrationssystem   (FIS)   der   FGG   Elbe: https://www.elbe-
494 datenportal.de/FisFggElbe/content/start/ZurStartseite.action;jsessionid=A37EDCF5B5EC1ECB15091447E64EC
495 538, last access: 21 November 2022.

496 Fraga, F., Ríos, A. F., Pérez, F. F., and Figueiras, F. G.: Theoretical limits of oxygen:carbon and oxygen:nitrogen
497 ratios during photosynthesis and mineralisation of organic matter in the sea, Sci. Mar., 62, 161–168,
498 https://doi.org/10.3989/scimar.1998.62n1-2161, 1998.

499 Garnier, J., Cébron, A., Tallec, G., Billen, G., Sebilo, M., and Martinez, A.: Nitrogen Behaviour and Nitrous Oxide
500 Emission in the Tidal Seine River Estuary (France) as Influenced by Human Activities in the Upstream Watershed,
501 Biogeochemistry, 77, 305–326, https://doi.org/10.1007/s10533-005-0544-4, 2006.

502 Gaumert, T. and Bergemann, M.: Sauerstoffgehalt der Tideelbe - Entwicklung der kritischen Sauerstoffgehalte im
503 Jahr 2007 und in den Vorjahren, Erörterung möglicher Ursachen und Handlungsoptionen,
504 Flussgebietsgemeinschaft Elbe, 2007.

505 Gonçalves, C., Brogueira, M. J., and Camões, M. F.: Seasonal and tidal influence on the variability of nitrous oxide
506 in the Tagus estuary, Portugal, Sci. Mar., 74, 57–66, https://doi.org/10.3989/scimar.2010.74s1057, 2010.

507 Halling-Sorensen, B. and Jorgensen, S. E. (Eds.): 3. Process Chemistry and Biochemistry of Nitrification, in:
508 Studies in Environmental Science, vol. 54, Elsevier, 55–118, https://doi.org/10.1016/S0166-1116(08)70525-9,
509 1993.

510 HAMBURG WASSER, Laurich, F.: pers. Comm.: N₂O in der Elbe, September 2022.

511 Hanke, V.-R. and Knauth, H.-D.: N₂O-Gehalte in Wasser-und Luftproben aus den Bereichen der Tideelbe und der
512 Deutschen Bucht, Vom Wasser, 75, 357–374, 1990.

513 Harley, J. F., Carvalho, L., Dudley, B., Heal, K. V., Rees, R. M., and Skiba, U.: Spatial and seasonal fluxes of the
514 greenhouse gases N₂O, CO₂ and CH₄ in a UK macrotidal estuary, Estuar. Coast. Shelf Sci., 153, 62–73,
515 https://doi.org/10.1016/j.ecss.2014.12.004, 2015.

516 Hedges, J. I. and Keil, R. G.: Sedimentary organic matter preservation: an assessment and speculative synthesis,
517 Mar. Chem., 49, 81–115, https://doi.org/10.1016/0304-4203(95)00008-F, 1995.

518 HPA and Freie und Hansestadt Hamburg: Deutsches Gewässerkundliches Jahrbuch - Elbegebiet, Teil III, Untere
519 Elbe ab der Havelmündung - 2014, Hamburg, 2017.

520 HPA, Karrasch, M.: pers. Comm.: Anfrage wegen N₂OPeak - Baggerarbeiten Elbe März 2021 und März 2022,
521 September 2022.

522 IPCC: Climate Change 2021: The Physical Science Basis. Contribution of Working Group I to the Sixth
523 Assessment Report of the Intergovernmental Panel on Climate Change, edited by: Masson-Delmotte, V., Zhai, P.,
524 Pirani, A., Connors, S. L., Péan, C., Berger, S., Caud, N., Chen, Y., Goldfarb, L., Gomis, M. I., Huang, M., Leitzell,
525 K., Lonnoy, E., Matthews, J. B. R., Maycock, T. K., Waterfield, T., Yelekçi, Ö., Yu, R., and Zhou, B., Cambridge
526 University Press, Cambridge, United Kingdom and New York, NY, USA,
527 https://doi.org/10.1017/9781009157896, 2021.

528 Johannsen, A., Dähnke, K., and Emeis, K.: Isotopic composition of nitrate in five German rivers discharging into
529 the North Sea, Org. Geochem., 39, 1678–1689, https://doi.org/10.1016/j.orggeochem.2008.03.004, 2008.

530 Kappenberg, J. and Fanger, H.-U.: Sedimenttransportgeschehen in der tidebeeinflussten Elbe, der Deutschen Bucht
531 und in der Nordsee, GKSS-Forschungszentrum, Geesthacht, 2007.

532 Kerner, M.: Interactions between local oxygen deficiencies and heterotrophic microbial processes in the elbe
533 estuary, Limnologica, 30, 137–143, https://doi.org/10.1016/S0075-9511(00)80008-0, 2000.

534 Knowles, R.: Denitrification, Microbiol. Rev., 46, 43–70, 1982.

535 Koch, M. S., Maltby, E., Oliver, G. A., and Bakker, S. A.: Factors controlling denitrification rates of tidal mudflats
536 and fringing salt marshes in south-west England, Estuar. Coast. Shelf Sci., 34, 471–485,
537 https://doi.org/10.1016/S0272-7714(05)80118-0, 1992.

538 Maavara, T., Lauerwald, R., Laruelle, G. G., Akbarzadeh, Z., Bouskill, N. J., Van Cappellen, P., and Regnier, P.:
539 Nitrous oxide emissions from inland waters: Are IPCC estimates too high?, Glob. Change Biol., 25, 473–488,
540 https://doi.org/10.1111/gcb.14504, 2019.

541 Middelburg, J. and Nieuwenhuize, J.: Uptake of dissolved inorganic nitrogen in turbid, tidal estuaries, Mar. Ecol.-
542 Prog. Ser., 192, 79–88, https://doi.org/10.3354/meps192079, 2001.

543 Middelburg, J. J. and Herman, P. M. J.: Organic matter processing in tidal estuaries, Mar. Chem., 106, 127–147,
544 https://doi.org/10.1016/j.marchem.2006.02.007, 2007.

545 Murray, R. H., Erler, D. V., and Eyre, B. D.: Nitrous oxide fluxes in estuarine environments: Response to global
546 change, Glob. Change Biol., 21, 3219–3245, https://doi.org/10.1111/gcb.12923, 2015.

547 Murray, R. H., Erler, D. V., Rosentreter, J., Wells, N. S., and Eyre, B. D.: Seasonal and spatial controls on N₂O
548 concentrations and emissions in low-nitrogen estuaries: Evidence from three tropical systems, Mar. Chem., 221,
549 103779, https://doi.org/10.1016/j.marchem.2020.103779, 2020.

550 Nevison, C., Butler, J. H., and Elkins, J. W.: Global distribution of N₂O and the ΔN₂O-AOU yield in the subsurface
551 ocean, Glob. Biogeochem. Cycles, 17, https://doi.org/10.1029/2003GB002068, 2003.

552 Nixon, S. W., Ammerman, J. W., Atkinson, L. P., Berounsky, V. M., Billen, G., Boicourt, W. C., Boynton, W. R.,
553 Church, T. M., Ditoro, D. M., Elmgren, R., Garber, J. H., Giblin, A. E., Jahnke, R. A., Owens, N. J. P., Pilson, M.
554 E. Q., and Seitzinger, S. P.: The fate of nitrogen and phosphorus at the land-sea margin of the North Atlantic
555 Ocean, Biogeochemistry, 35, 141–180, https://doi.org/10.1007/BF02179826, 1996.

556 Norbisrath, M., Pätsch, J., Dähnke, K., Sanders, T., Schulz, G., van Beusekom, J. E. E., and Thomas, H.: Metabolic
557 alkalinity release from large port facilities (Hamburg, Germany) and impact on coastal carbon storage,
558 Biogeosciences, 19, 5151–5165, https://doi.org/10.5194/bg-19-5151-2022, 2022.

559 Pätsch, A., Serna, A., Dähnke, K., Schlarbaum, T., Johannsen, A., and Emeis, K.-C.: Nitrogen cycling in the
560 German Bight (SE North Sea) — Clues from modelling stable nitrogen isotopes, Cont. Shelf Res., 30, 203–213,
561 https://doi.org/10.1016/j.csr.2009.11.003, 2010.

562 Pind, A., Risgaard-Petersen, N., and Revsbech, N. P.: Denitrification and microphytobenthic NO_3^- consumption
563 in a Danish lowland stream: diurnal and seasonal variation, Aquat. Microb. Ecol., 12, 275–284,
564 https://doi.org/10.3354/ame012275, 1997.

565 HAFEN HAMBURG: Willkommen auf der offiziellen Webseite des größten deutschen Seehafens:
566 http://www.portblog.de/de/startseite/, last access: 24 September 2021.

567 Quick, A. M., Reeder, W. J., Farrell, T. B., Tonina, D., Feris, K. P., and Benner, S. G.: Nitrous oxide from streams
568 and rivers: A review of primary biogeochemical pathways and environmental variables, Earth-Sci. Rev., 191, 224–
569 262, https://doi.org/10.1016/j.earscirev.2019.02.021, 2019.

570 Quiel, K., Becker, A., Kirchesch, V., Schöl, A., and Fischer, H.: Influence of global change on phytoplankton and
571 nutrient cycling in the Elbe River, Reg. Environ. Change, 11, 405–421, https://doi.org/10.1007/s10113-010-0152-
572 2, 2011.

573 Radach, G. and Pätsch, J.: Variability of continental riverine freshwater and nutrient inputs into the North Sea for
574 the years 1977–2000 and its consequences for the assessment of eutrophication, Estuaries Coasts, 30, 66–81,
575 https://doi.org/10.1007/BF02782968, 2007.

576 Redfield, A. C., Ketchum, B. H., and Richards, F. A.: The influence of organisms on the composition of sea-water,
577 Compos. Seawater Comp. Descr. Oceanogr. Sea Ideas Obs. Prog. Study Seas, 2, 26–77, 1963.

578 Rhee, T. S.: The process of air -water gas exchange and its application, Texas A&M University, College Station,
579 2000.

580 Rhee, T. S., Kettle, A. J., and Andreae, M. O.: Methane and nitrous oxide emissions from the ocean: A
581 reassessment using basin-wide observations in the Atlantic, J. Geophys. Res. Atmospheres, 114,
582 https://doi.org/10.1029/2008JD011662, 2009.

583 Robinson, A. D., Nedwell, D. B., Harrison, R. M., and Ogilvie, B. G.: Hypernutrified estuaries as sources of N_2O
584 emission to the atmosphere: the estuary of the River Colne, Essex, UK, Mar. Ecol. Prog. Ser., 164, 59–71, 1998.

585 Sanders, T., Schöl, A., and Dähnke, K.: Hot Spots of Nitrification in the Elbe Estuary and Their Impact on Nitrate
586 Regeneration, Estuaries Coasts, 41, 128–138, https://doi.org/10.1007/s12237-017-0264-8, 2018.

587 Schöl, A., Hein, B., Wyrwa, J., and Kirchesch, V.: Modelling Water Quality in the Elbe and its Estuary – Large
588 Scale and Long Term Applications with Focus on the Oxygen Budget of the Estuary, Küste 81 Model., 203–232,
589 2014.

590 Schroeder, F.: Water quality in the Elbe estuary: Significance of different processes for the oxygen deficit at
591 Hamburg, Environ. Model. Assess., 2, 73–82, https://doi.org/10.1023/A:1019032504922, 1997.

592 Siedler, G. and Peters, H.: Properties of sea water, Physical properties, in: Oceanography, vol. V/3a, edited by:
593 Sündermann, J., Springer, Berlin, Germany, 233–264, 1986.

594 Silvennoinen, H., Hietanen, S., Liikanen, A., Stange, C. F., Russow, R., Kuparinen, J., and Martikainen, P. J.:
595 Denitrification in the River Estuaries of the Northern Baltic Sea, AMBIO J. Hum. Environ., 36, 134–140,
596 https://doi.org/10.1579/0044-7447(2007)36[134:DITREO]2.0.CO;2, 2007.

20

597 Sommerfield, C. K. and Wong, K.-C.: Mechanisms of sediment flux and turbidity maintenance in the Delaware
598 Estuary, J. Geophys. Res. Oceans, 116, https://doi.org/10.1029/2010JC006462, 2011.

599 Tian, H., Xu, R., Canadell, J. G., Thompson, R. L., Winiwarter, W., Suntharalingam, P., Davidson, E. A., Ciais,
600 P., Jackson, R. B., Janssens-Maenhout, G., Prather, M. J., Regnier, P., Pan, N., Pan, S., Peters, G. P., Shi, H.,
601 Tubiello, F. N., Zaehle, S., Zhou, F., Arneth, A., Battaglia, G., Berthet, S., Bopp, L., Bouwman, A. F., Buitenhuis,
602 E. T., Chang, J., Chipperfield, M. P., Dangal, S. R. S., Dlugokencky, E., Elkins, J. W., Eyre, B. D., Fu, B., Hall,
603 B., Ito, A., Joos, F., Krummel, P. B., Landolfi, A., Laruelle, G. G., Lauerwald, R., Li, W., Lienert, S., Maavara,
604 T., MacLeod, M., Millet, D. B., Olin, S., Patra, P. K., Prinn, R. G., Raymond, P. A., Ruiz, D. J., van der Werf, G.
605 R., Vuichard, N., Wang, J., Weiss, R. F., Wells, K. C., Wilson, C., Yang, J., and Yao, Y.: A comprehensive
606 quantification of global nitrous oxide sources and sinks, Nature, 586, 248–256, https://doi.org/10.1038/s41586-
607 020-2780-0, 2020.

608 US EPA: Volunteer Estuary Monitoring: A Methods Manual, United States Environmental Protection Agency
609 (EPA), 2006.

610 Usui, T., Koike, I., and Ogura, N.: N_2O Production, Nitrification and Denitrification in an Estuarine Sediment,
611 Estuar. Coast. Shelf Sci., 52, 769–781, https://doi.org/10.1006/ecss.2000.0765, 2001.

612 Van Beusekom, J. E. E., Carstensen, J., Dolch, T., Grage, A., Hofmeister, R., Lenhart, H., Kerimoglu, O., Kolbe,
613 K., Pätsch, J., Rick, J., Rönn, L., and Ruiter, H.: Wadden Sea Eutrophication: Long-Term Trends and Regional
614 Differences, Front. Mar. Sci., 6, https://doi.org/10.3389/fmars.2019.00370, 2019.

615 Walter, S., Bange, H. W., and Wallace, D. W. R.: Nitrous oxide in the surface layer of the tropical North Atlantic
616 Ocean along a west to east transect, Geophys. Res. Lett., 31, L23S07, https://doi.org/10.1029/2004GL019937,
617 2004.

618 Weiss, R. F.: The solubility of nitrogen, oxygen and argon in water and seawater, Deep Sea Res. Oceanogr. Abstr.,
619 17, 721–735, https://doi.org/10.1016/0011-7471(70)90037-9, 1970.

620 Weiss, R. F. and Price, B. A.: Nitrous oxide solubility in water and seawater, Mar. Chem., 8, 347–359,
621 https://doi.org/10.1016/0304-4203(80)90024-9, 1980.

622 de Wilde, H. P. and de Bie, M. J.: Nitrous oxide in the Schelde estuary: production by nitrification and emission
623 to the atmosphere, Mar. Chem., 69, 203–216, https://doi.org/10.1016/S0304-4203(99)00106-1, 2000.

624 Winterwerp, J. C. and Wang, Z. B.: Man-induced regime shifts in small estuaries—I: theory, Ocean Dyn., 63,
625 1279–1292, https://doi.org/10.1007/s10236-013-0662-9, 2013.

626 WMO: Scientific Assessment of Ozone Depletion: 2018, World Meteorological Organization, Geneva,
627 Switzerland, 2018.

628 Wolfstein, K. and Kies, L.: Composition of suspended participate matter in the Elbe estuary: Implications for
629 biological and transportation processes, Dtsch. Hydrogr. Z., 51, 453–463, https://doi.org/10.1007/BF02764166,
630 1999.

631 Wrage, N., Velthof, G. L., van Beusichem, M. L., and Oenema, O.: The role of nitrifier denitrification in the
632 production of nitrous oxide, Soil Biol. Biochem., 33, 1723–1732, 2001.

633 ZDM, Wasserstraßen und Schifffahrtsverwaltung des Bundes: Abfluss - Neu Darchau, edited by: Wasserstraßen-
634 und Schifffahrtsamt Elbe, 2022.